Article

Piplartine Synthetic Analogs: In Silico Analysis and Antiparasitic Study against *Trypanosoma cruzi*

Rayanne H. N. Silva [1], Emanuel P. Magalhães [2], Rebeca C. Gomes [1], Yunierkis Perez-Castillo [3],
Alice M. C. Martins [2] and Damião P. de Sousa [1,*]

[1] Laboratory of Pharmaceutical Chemistry, Department of Pharmaceutical Sciences,
Federal University of Paraíba, João Pessoa 58051-900, Brazil; rayanne_nasci@hotmail.com (R.H.N.S.);
rebecagomes123456@gmail.com (R.C.G.)

[2] Postgraduate Program in Pharmaceutical Sciences, Faculty of Pharmacy, Dentistry and Nursing,
Federal University of Ceará, Fortaleza 60430-370, Brazil; emanuelpmagalhaes@gmail.com (E.P.M.);
martinsalice@gmail.com (A.M.C.M.)

[3] Facultad de Ingeniería y Ciencias Aplicadas, Área de Ciencias Aplicadas, Universidad de Las Américas,
Quito 170516, Ecuador; yunierkis@gmail.com

* Correspondence: damiao_desousa@yahoo.com.br

Abstract: Neglected tropical diseases (NTDs) cause thousands of deaths each year. Among these diseases, we find Chagas disease, whose etiologic agent is *Trypanosoma cruzi.* Piplartine is an alkamide present in various species of the genus *Piper* that possess trypanocidal activity. In this study, the antiparasitic potential of a collection of 23 synthetic analogs of piplartine against *Trypanosoma cruzi* was evaluated in vitro. The compounds were prepared via amidation and esterification reactions using 3,4,5-trimethoxybenzoic acid as starting material. The products were structurally characterized using ^{1}H and ^{13}C nuclear magnetic resonance, infrared spectroscopy, and high-resolution mass spectrometry. Of the twenty-three compounds tested in the cytotoxic activity assays, five presented good activity in the trypomastigote, epimastigote, and amastigote forms of *T. cruzi,* showing IC$_{50}$ values ranging from 2.21 to 35.30 μM, 4.06 to 34.30 μM, and 1.72 to 5.72 μM, respectively. *N-iso*-butyl-3,4,5-trimethoxybenzamide (**17**) presented potent trypanocidal activity with an IC$_{50}$ = 2.21 μM and selectively caused apoptosis (SI = 298.6). Molecular modeling experiments suggested the inhibitions of the histone deacetylase (HDAC) enzyme as the main trypanocidal mechanism of action of compound **17** in *T. cruzi.*

Keywords: piperlongumine; cytotoxicity; natural products; trypanocide; alkaloid; *Trypanosoma*; neglected diseases; antiparasitic activity

1. Introduction

Neglected tropical diseases (NTDs) present part of a varied group of protozoan, helminthic, bacterial, viral, fungal, and parasitic diseases [1,2]. Chagas disease (CD), a parasitosis caused by the hemoflagellate *Trypanosoma cruzi*, belongs to this group of tropical diseases and is also called American trypanosomiasis [3]. CD, in general, affects roughly six to seven million people worldwide (WHO, 2021) [4]. *T. cruzi* (Kinetoplastida) develops in blood-sucking insects of the Reduviidae family, in small wildlife mammals, and in humans [5,6]. This parasite is found in three main lifeforms: epimastigote (non-infective form found in invertebrate hosts), trypomastigote (the infective form of *T. cruzi*), and amastigote (replicative form in vertebrate hosts) [7].

CD is characterized as occurring in two phases: the first is the acute phase, being generally asymptomatic; for cases of symptomatic patients, the most frequent symptoms are: fever, lymphadenopathy, hepatosplenomegaly as well as inflammation at the site of inoculation. The second phase is called the chronic phase and leads to cardiomyopathy, gastrointestinal disturbances, or even death [8,9]. Current treatments involve the drugs

benznidazole and nifurtimox, yet possess low efficacy and can present many side effects [9]. Therefore, studies are needed to search for new chemical entities with therapeutic potential for the effective treatment of patients affected by this disease.

In drug candidate research, piplartine (Figure 1) has become increasingly relevant, as it is a natural substance found in the Piperaceae family (a kind of pepper). In the literature, there are already several studies where analogs of piplartine are synthesized and evaluated for different pharmacological activities, namely: antiparasitic, antitumor, and antimicrobial actions [10–12]. Of the antiparasitic activities, the most frequent studies are against *Trypanosoma* and *Leishmania* [10,13]. Investigation of its trypanocidal activity has been performed using structural analogs [14,15]. In the present work, we evaluated the trypanocidal potential of a collection of piplartine analogs against *Trypanosoma cruzi* trypomastigotes, epimastigotes, and amastigotes. An in silico approach was used involving structure–activity relationships to obtain chemical characteristics that might influence trypanocidal activity.
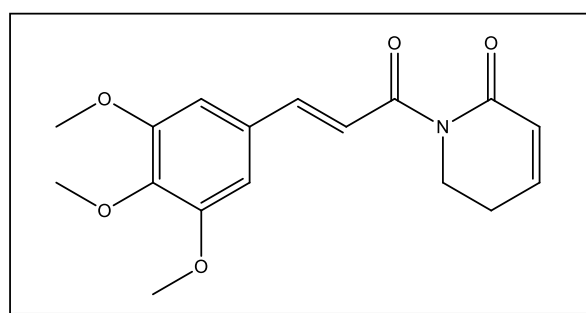

**Figure 1.** Chemical structure of piplartine.

2. Results

Products were obtained via four reaction approaches, as shown in Scheme 1: Fisher's esterification (a); esterification using alkyl or aryl halides (b); the Mitsunobu reaction (c); and coupling reactions using PyBOP (benzotriazol-1-yloxytripyrrolidinophosphonium hexafluorophosphate) (d) [11].

The analysis of ^{1}HNMR showed two aromatic hydrogens as singlets in δ_H from 7.20 to 7.36 ppm and signals of methoxy hydrogens in δ_H from 3.89 to 4.06 ppm. For the ^{13}CNMR, the common signals were δc from 165.7 to 166.7 ppm of C=O, signals in δc from 152.8 to 153.0 ppm and δc from 125.2 to 126.9 ppm, a signal at approximately a δc of 142.0 ppm, and a signal in δc from 106.7 to 107.0 ppm. In addition, the ^{13}CNMR spectrum shows signals in δc from 60.8 to 61.0 ppm and another signal with a chemical shift of δc from 56.0 to 56.4 ppm to carbons from methoxyl groups.

The compound 4-chloro-benzyl 3,4,5-trimethoxybenzoate (**9**) showed the following signals in the ^{1}H NMR: a multiplet to two hydrogens at δ 7.37–7.36 (H-3′, H-5′), another multiplet to two hydrogens at δ 7.36–7.35, (H-2′, H-6′), as well as a singlet to two hydrogens at δ 5.31 (H-7′) and a singlet signal at δ 7.31 ppm (H-2, H-6). For the ^{13}C NMR, we obtained a signal at 134.6 (C-1′), a second signal at 134.2 (C-4′) with the presence of the halogen (C–Cl), a signal to two carbons at 129.5 (C-2′, C-6′), another signal to two carbons at 128.7 (C-3′, C-5′), and a signal at 66.0 from C-7′. There were also signals from methoxy carbon (OCH$_3$) at δ 60.93 ppm and two methoxy carbons (2OCH$_3$) at δ 56.28 ppm.

For the compound 4-methylbenzyl 3,4,5-trimethoxybenzoate (**11**), the following ^{1}H NMR signals were obtained, referring to the aromatic substituent: a doublet to two protons at δ 7.34 (*d*, *J* = 8.0 Hz, H-3′, H-5′), another doublet to two hydrogens at δ 7.20 (*d*, *J* = 8.4 Hz, H-2′, H-6′), a singlet to two protons at δ 5.32 (H-7′), and another singlet at δ 2.36 (s, 3H, H-8′) referring to methyl hydrogens in the *para* position of the aromatic ring, and a singlet signal at δ 7.32 ppm (H-2, H-6). In the ^{13}C NMR, a signal at 138.1 (C-4′), another signal at 133.1 (C-1′), a signal to two carbons at 129.2 (C-3′, C-5′), another signal to two carbons at 128.4 (C-2′, C-6′), a signal at 66.7 (C-7′), and a signal at 21.3 referring to methyl in the

para position. In addition, there were signs from methoxy carbon (OCH$_3$) at δ 60.85 ppm and two methoxy carbons (2OCH$_3$) at δ 56.16 ppm.
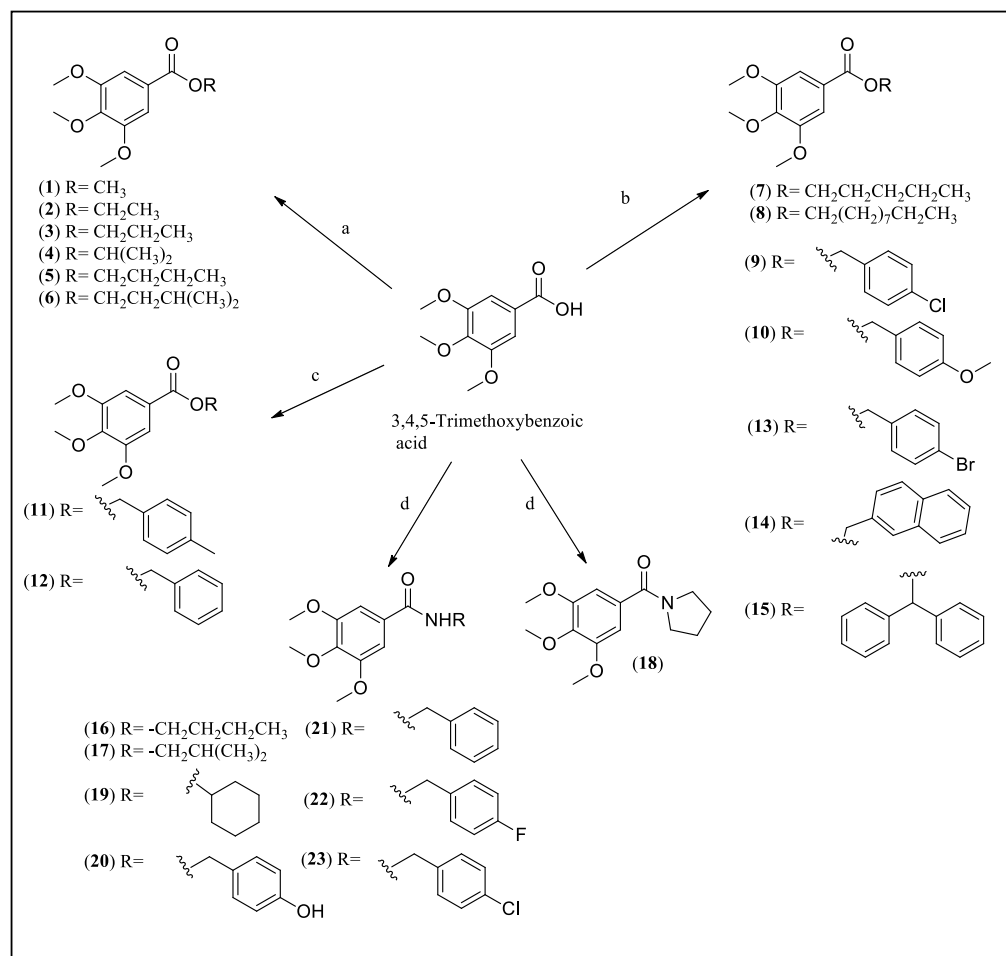
Scheme 1. Synthesis of **1–23**. Reaction conditions: (**a**) ROH, H$_2$SO$_4$, reflux; (**b**) halide, Et$_3$N, acetone, 60 °C, reflux; (**c**) ROH, THF, TPP, DEAD, 0 °C to r.t; (**d**) RNH$_2$ or pyrrolidine, DMF, PyBOP, Et$_3$N, CH$_2$Cl$_2$, 0 °C to r.t. Yield variation: 29.8 to 99.6%.

The analyses from IR spectroscopy showed common signals above 3000 cm^{-1} (C–H sp2 stretch), signals at 1600 and 1475 cm^{-1} from the aromatic ring, bands of carbonyl from 1740 to 1715, and 1300 to 1000 cm^{-1} (C–O stretch). The methoxyls had signals from 1250 to 1040 cm^{-1} (aryl ether stretch). The amides showed a band at approximately 3300 cm^{-1} (-NH), except amide **18**, and a band from 1680 to 1630 cm^{-1} of stretching C=O. The unpublished compounds were also analyzed by HRMS (FT-ICR) spectrometry [11].

The trypanocidal effects of compounds **15–18** and **20** against *Trypanosoma cruzi* (trypomastigote and epimastigote forms) are shown in Table 1.

Cytotoxic evaluation of the 23 derivatives was performed in LLC-MK2 host cells submitted to the MTT (3,4,5-dimethiazol-2,5-diphenyltetrazoliumbromide) reduction assay. Cell viability values are shown in Table 1. Antiparasitic assays were also performed with the less cytotoxic derivatives, and the analogs **15–18** and **20** (presenting low cytotoxicity towards healthy cells) were selected for further testing.

The cell death study is shown in Figure 2, which contains the scatter plot density graphs of the cells.

Table 1. Cell viability and trypanocidal activity of 3,4,5-trimethoxybenzoic acid derivatives against *Trypanosoma cruzi* (trypomastigote, epimastigote, and amastigote forms).

Compound	Y Strain (Trypomastigotes) (IC_{50} μM)	Y Strain (Epimastigotes) (IC_{50} μM)	Y Strain (Amastigotes) (IC_{50} μM)	Cell Viability (LLC-MK2) (CC_{50} μM)	S.I. (Trypomastigotes)	S.I. (Amastigotes)
1	-	-	-	155.56 ± 25.20	-	-
2	-	-	-	294.65 ± 37.79	-	-
3	-	-	-	144.41 ± 14.20	-	-
4	-	-	-	>488.70	-	-
5	-	-	-	380.16 ± 63.17	-	-
6	-	-	-	81.89 ± 11.12	-	-
7	-	-	-	296.63 ± 63.33	-	-
8	-	-	-	291.09 ± 38.92	-	-
9	-	-	-	375.98 ± 141.08	-	-
10	-	-	-	118.73 ± 24.46	-	-
11	-	-	-	37.06 ± 18.97	-	-
12	-	-	-	154.11 ± 20.51	-	-
13	-	-	-	141.47 ± 30.22	-	-
14	-	-	-	225.90 ± 72.40	-	-
15	35.30 ± 6.18	24.47 ± 2.96	4.30 ± 3.69	>528.51	>14.97	290.43
16	6.21 ± 0.86	10.66 ± 3.40	5.72 ± 1.61	659.13 ± 222.57	106.14	115.16
17	2.21 ± 0.37	8.71 ± 2.24	1.72 ± 0.15	659.13 ± 195.27	298.64	383.04
18	8.14 ± 1.70	34.30 ± 12.89	3.96 ± 0.22	676.59 ± 142.10	83.10	170.95
19	-	-	-	513.02 ± 177.32	-	-
20	8.95 ± 1.98	4.06 ± 0.63	3.06 ± 0.53	>630.26	>70.42	279.17
21	-	-	-	305.58 ± 45.63	-	-
22	-	-	-	343.13 ± 121.03	-	-
23	-	-	-	157.78 ± 22.22	-	-
Benznidazole	161.40 ± 31.80	115.10 ± 16.32	-	502.60 ± 57.80	3.11	-

Legend—the assays were carried out in triplicate (n = 3). All data are reported as mean ± standard error mean (SEM). Selectivity index (S.I.) = IC_{50} (trypomastigote or amastigote forms)/CC_{50} (LLC-MK2).

Flow cytometry assays with Rho 123 (rhodamine 123) are shown in Figure 3.

In the flow cytometry assays, the epimastigote forms of *T. cruzi* were used, and the cells were divided into four cell populations: viable cells, with low levels of labeling for both fluorochromes (un-labeled); necrotic cells, labeled only with 7-AAD (7AAD+) (7-Aminoactinomycin D); apoptotic cells, labeled with annexin V-PE only (/AxPE+); and doubly labeled late apoptotic cells (7AAD+/AxPE+) [16].

Cells were incubated with compounds **15–18** and **20** for 24 h at concentrations of equivalent to IC_{50} and $2 \times IC_{50}$. In this assay, a reduction in the percentage of viable cells and an increase in the percentage of 7-AAD-labeled cells were observed, indicating cell death by necrosis (Figure 2). Necrosis results in irreversible cell injury with loss of cell membrane integrity [17]. The increase is also observed in the displacement of cell populations, as shown in Figure 2.
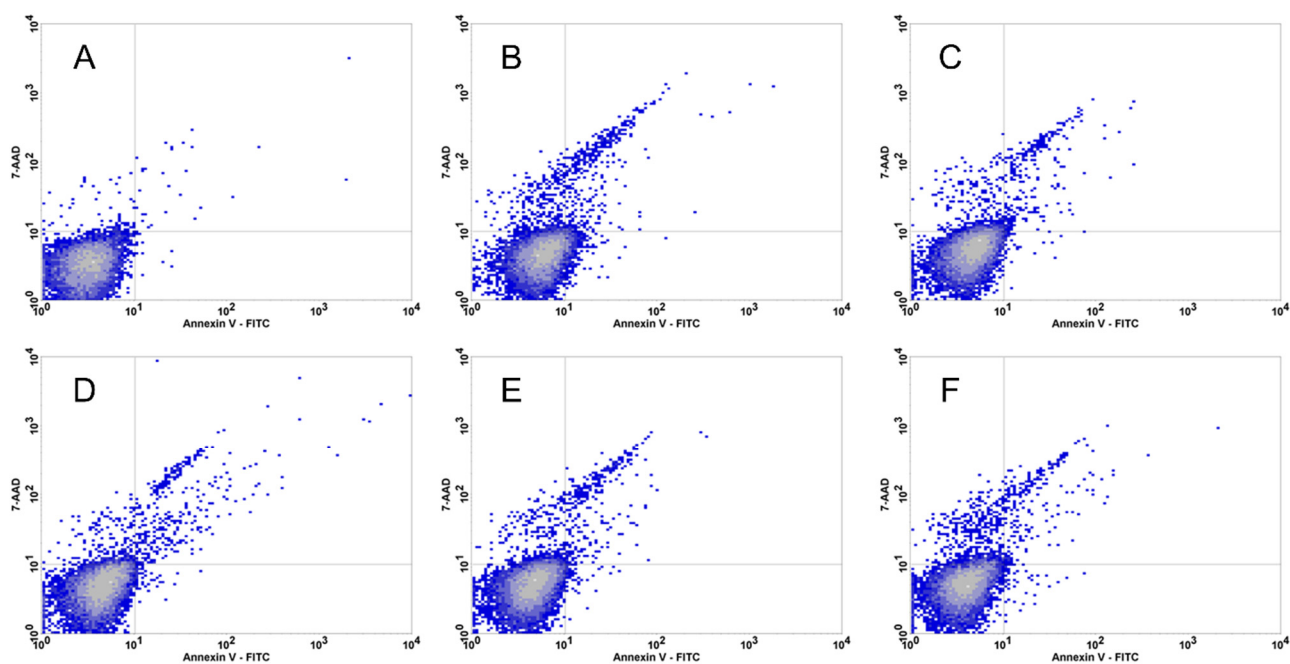
Figure 2. Scatter plots of cells from the cell death study. (**A**) Control group; (**B**) group treated with compound **16**; (**C**) group treated with compound **17**; (**D**) group treated with compound **18**; (**E**) group treated with compound **20**; (**F**) group treated with compound **15**.

Flow cytometry assays with Rho 123 (rhodamine 123) were also performed to evaluate the mitochondrial transmembrane potential of the epimastigotes treated with the derivatives. As shown in Figure 3, treatment with the compounds at both concentrations was able to markedly reduce epimastigote mitochondrial capacity. The derivatives that presented the best reductions were compounds **15**, **17**, and **20** at 36%, 37%, and 43%, respectively.

Modeling studies were performed to investigate the possible trypanocidal mechanism of action of compound **17**. Initially, potential targets for the compound were identified using a homology-based target fishing approach. Then, the compound was docked to each of its predicted targets to produce binding hypotheses. The free energies of binding are finally predicted for these protein–compound **17** complexes using an approach that bases on MD simulations. These MD-derived energies of binding are the criteria for prioritizing the possible mechanism of action of the compound. In this way, we avoid relying on molecular docking results that use simplified scoring functions designed to process large amounts of compounds in a reasonable time, and scoring values should not be compared across different molecular targets.

Computational target fishing approaches are based on the similarity principle, which states that similar chemical compounds should have similar bioactivity profiles. These methods are often trained with activity data available on public databases such as ChEMBL. Unfortunately, such databases are biased toward interactions of chemicals with human proteins. Thus, in this study, all probable targets of compound **17** are first predicted, and the homolog proteins of these in *T. cruzi* are identified. In this way, we address the limitations in bioactivity data deposited in the databases for the parasite while narrowing the space of possible molecular targets of the compounds in *T. cruzi*. This approach serves to propose an initial set of possible targets of the compound for further molecular docking calculations and MD simulations.

Table 2 lists the potential molecular targets of compound **17** in *T. cruzi* that were identified using the homology-based target fishing approach. The information in Table 2 includes the UniProt accession number, the ID used in the manuscript, and a brief functional description for each protein. Compound **17** was docked to the proteins listed in Table 2 using the methodology described in the Materials and Methods section. In the case of

the DHFR–TS enzyme, both the folate and dUMP were explored separately. On the other hand, TUBA and TUBB polymerize to form microtubules, and the inhibition of this process can influence the normal development of cells. Thus, the binding of compound **17** to the interface of the TUBA–TUBB dimer was explored. The assembly of this dimer was carried out as proposed in a previous report [18] and will be referred to as TUB from here on. The molecular docking results are provided in Table 3.
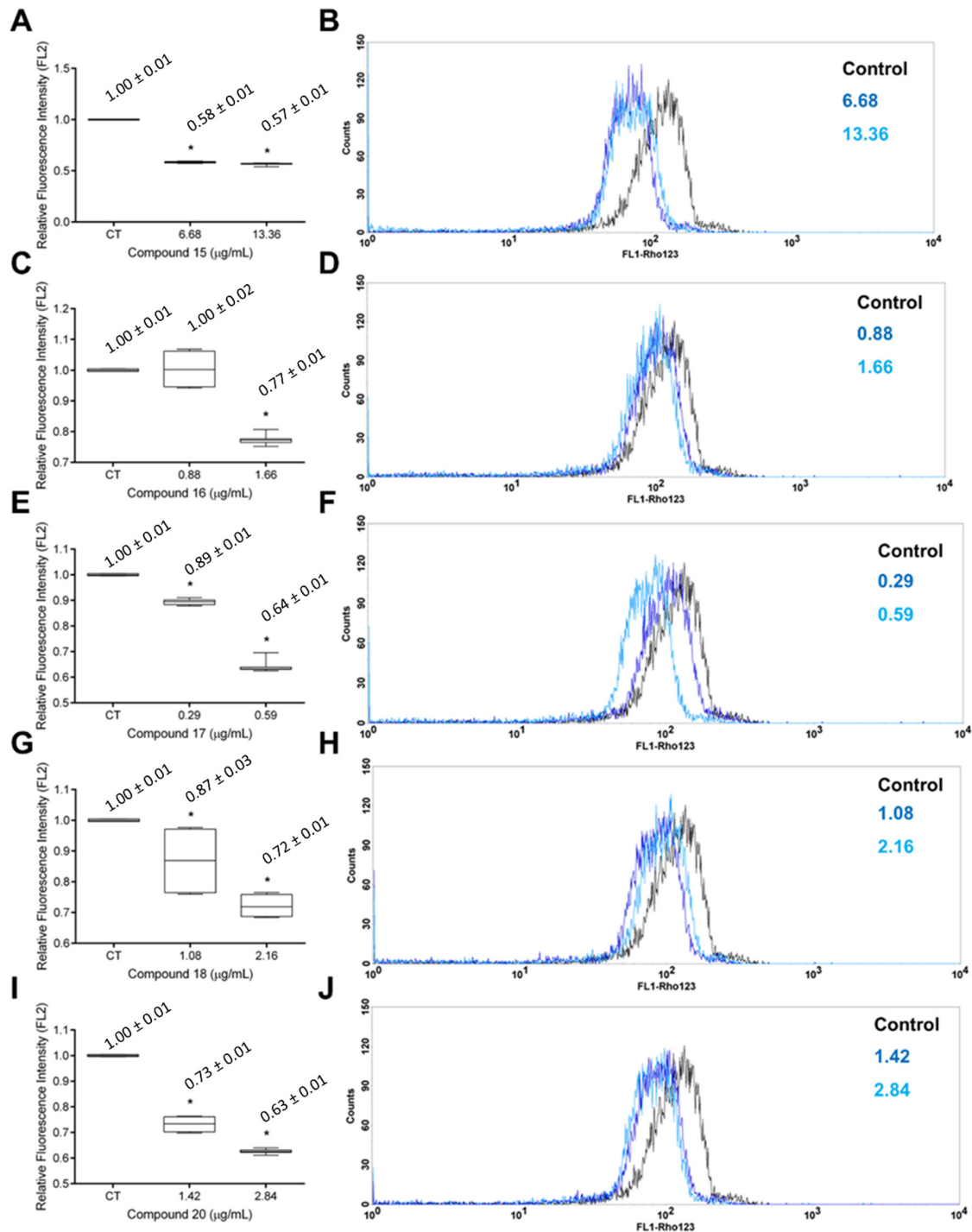

Figure 3. Relative fluorescence intensity box plot (**A,C,E,G,I**) and histogram graphs (**B,D,F,H,I**) of Rho123 dye in epimastigote forms treated with compounds **15** (**A,B**), **16** (**C,D**), **17** (**E,F**), **18** (**G,H**) and **20** (**I,J**). The black, dark blue, and light blue lines represent the fluorescence of the control groups, the highest, and the lowest compound concentrations, respectively. * $p < 0.05$ vs. control group.

Table 2. Potential molecular targets of compound **17** in *T. cruzi*.

UniProt Accession	ID	Description
Q4DFL5	PPI-1	Peptidylprolyl isomerase
Q4D5W5	PPI-2	Peptidylprolyl isomerase
Q4DQU7	HDAC	Histone deacetylase
Q4D3A0	MAPK-1	Mitogen-activated protein kinase
A0A2V2VTR7	MAPK-2	Mitogen-activated protein kinase
Q4D2F2	IleRS	Isoleucine-tRNA ligase
Q4DQP2	TUB-B	Tubulin beta chain
Q4CLA1	TUB-A	Tubulin alpha chain
Q4D397	PDE	Phosphodiesterase
Q4DLS1	DHFR–TS	Bifunctional dihydrofolate reductase–thymidylate synthase

Table 3. Results of docking compound **17** to its potential targets.

Target	Pose	PLP [a]	Z_PLP [b]	GS [c]	Z_GS [d]	CS [e]	Z_CS [f]	ASP [g]	Z_ASP [h]	Aggregated Score
PPI-1	1	56.15	2.28	18.93	0.54	26.55	1.85	32.06	1.31	1.49
	2	48.94	0.22	17.9	0.46	26.35	1.78	33.92	1.88	1.08
	3	49.73	0.45	22.1	0.79	22.96	0.51	35.91	2.5	1.06
PPI-2	1	59.08	0.99	25.08	0.72	25.82	0.65	40.92	0.89	0.81
HDAC	1	69.37	2.25	16.18	0.75	23.07	2.13	30.07	0.65	1.44
	2	66.41	1.66	14.14	0.68	22.5	1.92	30.99	0.81	1.27
	3	66.06	1.6	30.16	1.25	20.27	1.11	31.16	0.84	1.2
MAPK-1	1	55.16	3.18	15.68	0.81	18.62	1.44	29.28	3.12	2.14
MAPK-2	1	59.91	2.29	25.5	1.09	23.16	1.58	30.56	1.42	1.6
	2	57.54	1.79	23.44	0.96	22.64	1.41	33.64	2.16	1.58
	3	54.12	1.06	22.41	0.89	21.46	1.04	34.22	2.29	1.32
	4	55.86	1.43	24.66	1.04	21.02	0.9	27.56	0.71	1.02
IleRS	1	44.64	2.02	−1.38	0.43	18.5	3.24	29.06	1.55	1.81
TUB	1	36.01	1.69	−11.12	0.37	12.91	2.03	18.36	1.99	1.52
PDE	1	61.37	2.72	13.71	0.59	21.22	0.45	32.11	0.82	1.15
	2	52.05	0.48	18.63	0.75	24.07	2.3	31.82	0.73	1.06
DHFR–TS (folate site)	1	55.63	1.91	13.93	0.96	20.24	1.79	29.19	2.49	1.79
	2	56.42	2.2	−23.3	−0.98	20.91	2.18	27.15	1.88	1.32
DHFR–TS (dUMP site)	1	35.43	0.69	8.3	0.69	8.18	0.25	22.22	2.99	1.15
	2	37.56	1.24	18.44	1.4	12.49	1.9	11.47	0.01	1.14

[a] PLP score, [b] scaled PLP score, [c] GoldScore score, [d] scaled GoldScore score, [e] ChemScore score, [f] scaled ChemScore score, [g] ASP score, [h] scaled ASP score.

Molecular docking resulted in 20 different compound–receptor complexes that were then subject to the calculation of the MD-based free energies of binding according to the procedure described in the Section 4. The results of these calculations are given as Supplementary Materials in Table S1, while the lowest (best) free energy of binding computed for compound **17** to each target is represented in Figure 4.

According to these results, the most probable target of the chemical in *T. cruzi*, among those evaluated in our research, is HDAC (histone deacetylase). Hence, a more detailed analysis of the predicted binding mode of compound **17** to HDAC was performed, as shown in Figure 5. For this enzyme, the ligand is predicted to orient with the tri-methoxyphenyl ring at the entrance of the binding cavity, forming π–π stacking interactions with F152 and H180 while also interacting with F208 and L274. The carbonyl oxygen points directly to the Zn^{2+} ion. On the other hand, the amide nitrogen serves as a hydrogen bond donor to G151. These π–π stacking, electrostatic, and hydrogen bond interactions are proposed as the main factors stabilizing the binding of compound **17** to HDAC. Finally, the isobutyl tail

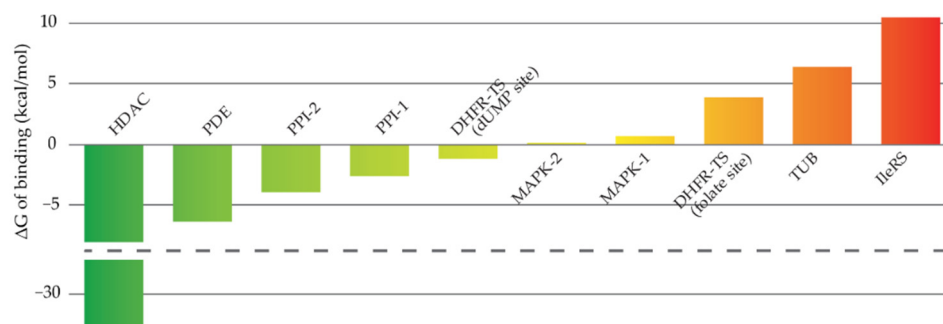of the ligand occupies the bottom of the binding cavity, a region lined by A32, M33, H143, G151, C153, and G304.

Figure 4. Free energies of binding of compound **17** to its potential molecular targets.
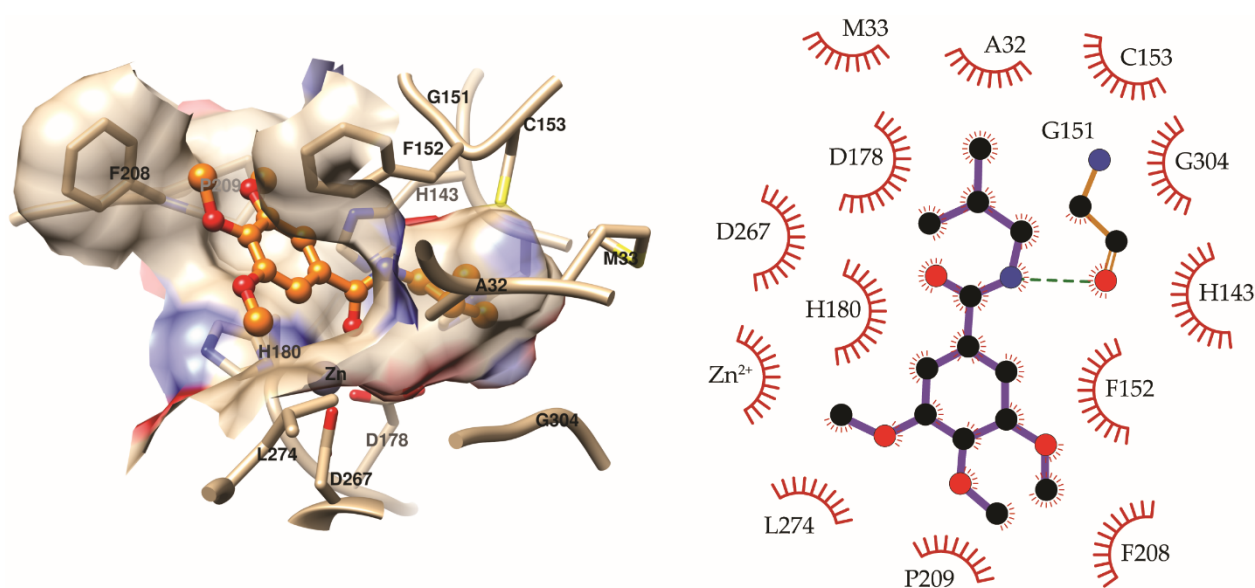

Figure 5. Predicted binding conformation of compound **17** to HDAC. The represented ligand conformation is the centroid of the most populated cluster obtained after clustering the ligand conformations in the 100 MD snapshots used for MM-PBSA calculations. The compound is represented as orange balls and sticks. Only residues interacting with the ligand in at least 50% of the analyzed MD snapshots are labeled and included in the interactions diagram. The figure was produced with UCSF Chimera [19] and LigPlot+ [20].

In addition to its potential targets, the ADME properties of compound **17** and the reference compound benznidazole were computed with the SwissADME [21] web server. The results of these predictions are provided in Table 4 and show that **17** has favorable physicochemical properties for oral bioavailability. In contrast, benznidazole contains fewer insaturations than required for oral bioavailability. On the other hand, compound **17** is less soluble in water and more lipophilic than benznidazole. Both compounds are predicted with high gastrointestinal absorption and as nonsubstrates of P-gp. One property that needs to be modified in compound **17** is its ability to cross the blood–brain barrier. Finally, the ADME predictions show that the cytochrome inhibitory profile of **17** must be improved in future rounds of joint bioactivity and ADME properties optimization.

Table 4. ADME predictions for compound **17** and the reference drug benznidazole.

Parameter	Compound 17	Benznidazole
Physiochemical properties		
Molecular weight (g/mol)	267.32	260.25
Rotatable bonds	7	6
H-bond acceptors	4	4
H-bond donors	1	1
Fraction Csp3	0.5	0.17
TSPA (A^2)	56.79	92.74
Lipophilicity (Log $P_{o/w}$)		
iLOGP	3.01	1.15
XLOBP3	2.44	0.91
MLOGP	1.5	0.37
Consensus	2.31	0.49
Solubility		
Water solubility	Moderately soluble	Soluble
Pharmacokinetics		
Gastrointestinal absorption	High	High
Skin permeability (Log K_P, cm/s)	−6.2	−7.24
Blood–brain permeability	Yes	No
P-gp substrate	No	No
CYP1A2 inhibitor	Yes	No
CYP2C19 inhibitor	No	No
CYP2C9 inhibitor	No	No
CYP2D6 inhibitor	Yes	No
CYP3A4 inhibitor	No	No

3. Discussion

Analysis of the biological activity of the 3,4,5-trimethoxybenzoic acid derivatives was performed using the results obtained in the antiparasitic assays (IC_{50}). Twenty-three compounds were tested at CC_{50} against LLC-MK2 cells, of which five analogs (one ester and four amides) were selected for IC_{50} assays. In the evaluation of trypanocidal activity against the trypomastigote form, amides **16**–**18** and **20** were more potent than the ester compound **15**.

N-butyl-3,4,5-trimethoxybenzamide amide (**16**) and *N-iso*-butyl-3,4,5-trimethoxybenzamide amide (**17**) presented IC_{50} of 6.21 μM and 2.21 μM, respectively; and SI = 83.10 and 298.64. The isomerism of these compounds reveals that compound **16** presents a linear side carbon chain as a substituent, while compound **17** presents a branched side carbon chain. The greater volume of this alkyl substituent results in the potentiation of trypanocidal action against the trypomastigote form, in addition to presenting a high selectivity index for this strain. The compound *N*-pyrrolidyl-3,4,5-trimethoxybenzamide (**18**) presented an IC_{50} of 8.14 μM, while the analog *N*-4-hydroxybenzyl-3,4,5-trimethoxybenzamide (**20**) presented an IC_{50} of 8.95 μM. Thus, these compounds showed similar activity, despite having different substituents.

The obtained results corroborate with those from Mengarda and collaborators (2020) [22], who tested piplartine in vitro and in vivo for antiparasitic activity. In the in vivo study, treatment with the highest dose of piplartine (400 mg/kg) significantly reduced the total load of the etiological agent, which for this study was *Schistosoma mansoni*, demonstrating satisfactory results in the tests, and suggesting that piplartine may be useful as a prototype in the development new antiparasitic agents.

The ester diphenyl 3,4,5-trimethoxybenzoate (**15**) presented the highest IC_{50} (35.30 μM) of the five bioactive analogs tested, being the least potent compound in the group against the trypomastigote form. In the study by Nobrega et al. (2019) [10], where piplartine analogs were also tested, the antiparasitic results were better for the ester compounds. For example, benzyl 3,4,5-trimethoxybenzoate (IC_{50} = 0.025 ± 0.009 μM, SI > 3.2) presented

the best activity against *Leishmania amazonensis*. In this study, the results show that the benzamides showed a better antiparasitic profile against *T. cruzi*.

Evaluating the results obtained against the epimastigote form, compound **16** presented an IC_{50} of 10.66 μM, while compound **17** presented an IC_{50} of 8.71 μM, confirming that branched substituents present greater trypanocidal activity. Comparing compound **18** with compound **20**, presenting IC_{50} of 34.30 μM and 4.06 μM, respectively, compound **20** was about 8.4 times more potent. In this case, against the epimastigote form, amides with aryl side chains present greater cytotoxicity than those with cyclic chains. Comparing amide **20** with the ester compound **15**, both present a side chain formed by aromatic rings, presenting IC_{50} values of 4.06 μM and 24.47 μM, respectively. It was evident that the amide was more potent than the ester and may show more promising results for the epimastigote form.

Cotinguiba et al. (2009) [23] isolated piperamides from *Piper tuberculatum*, and derivatives of these molecules were investigated for their trypanocidal activity. Of the fourteen compounds tested, piplartine was the most potent in inhibiting the growth of epimastigotes with an IC_{50} = 10.5 μM. It can therefore be suggested that piplartine and its derivatives are promising molecules for trypanocidal activity.

Analyzing the data obtained against the amastigote form, amide **16** presented an IC_{50} of 5.72 μM, while amide **17** proved to be more potent with an IC_{50} of 1.72 μM, which is the best result for this evolutionary form of *T. cruzi* and suggests that, in fact, branched substituents result in greater trypanocidal potency in addition to a higher selectivity index (SI = 383.0). Comparing amide **18** with amide **20**, they showed a similar IC_{50}, being 3.96 and 3.06 μM, respectively; even with different substituents (alkyl and aryl), there was no difference in potency. Comparing amide **20** with ester **15**, since both have substituted aryl, presenting IC_{50} 3.06 and 4.30 μM, respectively, thus observing similar bioactivity, differing from the other evolutionary forms (trypomastigote and epimastigote) that the amide presented greater potency.

The predicted potential targets for compound **17** cover diverse functions such as protein folding, the deacetylation of acetyl-lysine substrates, protein kinases, attachment of isoleucine to tRNA, cell structure, the regulation of the levels of cAMP and cGMP, as well as the production of tetrahydrofolate. From the modeling results, it was observed that the most probable target of compound 17 in *T. cruzi* is the HDAC enzyme.

The proposed mechanism of action could explain the trypanocidal activity of compound **17**. HDAC inhibitors are currently being investigated for their potential as antitrypanosomal drugs [24]. In this sense, diverse HDAC inhibitors have been reported as effective and selective against *T. cruzi* and proposed as starting points for future activity optimization [25]. Additional research efforts should be directed to evaluate the predicted HDAC inhibitory activity of compound **17** in *T. cruzi*. Finally, the modeling results presented herein can serve to guide the future optimization of benzamide derivatives as trypanocidal agents.

4. Materials and Methods

4.1. Chemistry

The reagents and silica gel 60, ART 7734 in column chromatography used were obtained from Sigma-Aldrich. The ^{1}HNMR and ^{13}CNMR spectra were obtained in Bruker Avance III HD spectrometers operating at 400 MHz and 100 MHz and with a Varian NMR operating at 500 MHz and 125 MHz. The multiplicities of the ^{1}HNMR were as follows: *s* (singlet), *d* (doublet), *t* (triplet), *qu* (quintet), *sext* (sext), *sept* (septet), and *m* (multiplet). Chemical shifts were presented in ppm (parts per million). The Fourier-transform infrared spectroscopy used an Agilent Technologies Cary 630 FTIR instrument. High-resolution mass spectrometry was performed at the Biomolecules Mass Spectrometry Center-UFRJ using the spectrometer Solarix XR—FT-ICR configuration (Bruker) with an electrospray ionization source, positive mode. The Microquímica apparatus, Model MQAPF 302, Palhoça, Brazil, was used to measure melting points. The Rf calculations and analysis of the reaction products occurred via silica gel sheet chromatograph from Merck (silica 60, F 254) [11].

4.1.1. Preparation of Compounds **1–6**

3,4,5-trimethoxybenzoic acid (0.1 g; 0.47 mmol), 20 mL of alcohol, and sulfuric acid (0.2 mL) were added into a 50 mL flask. The reaction mixture was refluxed under magnetic stirring for 5 to 24 h. The products were purified by column chromatography using silica gel [11,26,27].

4.1.2. Preparation of Compounds **7–10** and **13–15**

Into a 50 mL flask containing one equivalent of 3,4,5-trimethoxybenzoic acid and 15 mL of anhydrous acetone, four equivalents of triethylamine and one equivalent of halide were added. The reaction mixture was conducted under reflux and magnetic stirring for 72 h. The products were purified by column chromatography using silica gel [11,26,28].

4.1.3. Preparation of Compounds **11** and **12**

A solution was prepared containing 3,4,5-trimethoxybenzoic acid 1 eq. (100 mg; 0.47 mmol) and 1 eq. of alcohol (0.47 mmol) solubilized in 4 mL of tetrahydrofuran (THF) at 0 °C. After 30 min, 1 eq. triphenylphosphine (TPP) and 1 eq. of diisopropyl azodicarboxylate (DEAD) were added. The reaction was conducted under constant magnetic agitation at ambient temperature for 72 h. The products were purified by column chromatography using silica gel [11,26].

4.1.4. Preparation of Compounds **16–23**

3,4,5-trimethoxybenzoic acid (0.1 g; 0.47 mmol), 0.47 mmol of amine solubilized in dimethylformamide (1.0 mL; 0.94 mmol), and triethylamine (0.06 mL; 0.47 mmol) at 0 °C were added into a 50 mL flask. After 30 min, PyBOP (0.24 g; 0.47 mmol) in dichloromethane (1.0 mL) was added under magnetic stirring. The reaction mixture was carried out at room temperature for 6 to 24 h. The products were purified by column chromatography using silica gel [11,26,29–31].

4-Chlorobenzyl 3,4,5-trimethoxybenzoate (**9**): colorless crystalline solid, yield 42.9% (69.7 mg; 0.20 mmol); M.P., 108–109 °C; TLC (8:2 hexane/AcOEt), Rf = 0.44; IR υmax (KBr, cm^{-1}): 3008 (C–H sp^2 $_{AROMÁTICO}$), 2960, 1713, 1664, 1595 and 1472, 1335 and 1133, 1229 and 1092, 1006, 805; ^{1}H NMR (400 MHz, CDCl$_3$): δ 7.37–7.36 (*m*, 2H, H-3′, H-5′); 7.36–7.35 (*m*, 2H, H-2′, H-6′); 7.31 (*s*, 2H, H-2, H-6); 5.1 (*s*, 2H, H-7′); 3.89 (*s*, 9H, 3-MeO, 4-MeO, 5-MeO) ppm; ^{13}C NMR (100 MHz, CDCl$_3$): δ 166.0; 153.0; 142.5; 134.6; 134.2; 129.4; 128.7; 124.8; 106.9; 66.0; 60.9; 56.2 ppm. HRMS (FT-ICR) analysis: C$_{17}$H$_{17}$O$_5$ calculated theoretical value [M + H]$^+$, 337.0837; found, 337.0836.

4-Methylbenzyl 3,4,5-trimethoxybenzoate (**11**): colorless crystalline solid, yield 33.3% (49.7 mg; 0.15 mmol); M.P., 93–94 °C; TLC (8:2 hexane/AcOEt), Rf = 0.5; IR υmax (KBr, cm^{-1}): 3015, 2971, 1708, 1666, 1590 and 1467, 1334 and 1127, 1229 and 1008, 812; ^{1}H NMR (400 MHz, CDCl$_3$): δ 7.34 (*d*, *J* = 8.0 Hz, 2H, H-3′, H-5′); 7.32 (*s*, 2H, H-2, H-6); 7.20 (*d*, *J* = 8.4 Hz, 2H, H-2′, H-6′); 5.32 (*s*, 2H, H-7′); 3.89 (*s*, 9H, 3-MeO, 4-MeO, 5-MeO); 2.36 (*s*, 3H, H-8′) ppm; ^{13}C NMR (100 MHz, CDCl$_3$): δ 166.1; 152.9; 142.3; 138.1; 133.1; 129.2; 128.4; 125.2; 107.0; 66.7; 60.8; 56.2; 21.3 ppm. HRMS (FT-ICR) analysis: C$_{18}$H$_{20}$O$_5$ calculated theoretical value [M + H]$^+$, 317.1383; found, 317.1382.

4.2. Cytotoxic Activity

4.2.1. Collection and Preparation of Cells

The cytotoxicity of the 3,4,5-trimethoxybenzoic acid derivatives was evaluated in LLC-MK2 cells with the aim of analyzing their selectivity for *T. cruzi* in relation to host cells. LLC-MK2 cells (ATCC CCL-7) are a lineage of epithelial cells obtained from the renal tubules of monkeys (*Macaca mulatta).* The cells were obtained from the Rio de Janeiro Cell Bank (BCRJ) and cultivated in DMEM medium (Dulbecco's Modified Eagle's Medium, pH 7.4)—supplemented with 10% FBS (fetal bovine serum) and the antibiotics (penicillin—200 UI·mL^{-1} and streptomycin—130 mg·mL^{-1}). The epimastigote forms (Y strain) of *T. cruzi* were provided by the Parasite Biochemistry Laboratory of the Uni-

versity of São Paulo (USP) and cultivated in LIT medium (*Liver Infusion Tryptose,* with NaCl 4 gL^{-1}; $Na_2HPO_4.12H_2O$ 11.6 gL^{-1}; KCl 0.4 gL^{-1}; glucose 2.2 gL^{-1}; tryptose 5 gL^{-1}; liver infusion 5 gL^{-1}; and bovine hemin 25 $mg·L^{-1}$ at pH 7.4), supplemented with 10% FBS, and the antibiotics (penicillin—200 $IU·mL^{-1}$ and streptomycin—50 $mg·L^{-1}$). The cultures were maintained at 28 ± 1 °C in a BOD (*Biochemical Oxygen Demand*) oven in sterile bottles [32]. The trypomastigote forms of *T. cruzi* were obtained from host cell infections [33]. For this, LLC-MK2 cells were cultured in sterile 25 cm^2 bottles at a concentration of 1×10^5 $cells·mL^{-1}$ in DMEM 10% FBS medium. After 48 h of incubation in a CO_2 oven, the medium was replaced by DMEM 2% FBS without antibiotics, and the cells were infected with trypomastigotes at a rate of 20 parasites per cell. To evaluate the effect on intracellular amastigotes, LLC-MK2 cells (10^5 $cells·mL^{-1}$) were cultured in 24-well plates on 13 mm diameter sterile coverslips for 24 h incubated in a CO_2 oven. The cells were then infected with trypomastigotes (2×10^6 $cells·mL^{-1}$) and incubated for 48 h. They were then further treated with Ch-DiCl (150, 75, 37.5, and 18.75 μM) and kept in a CO_2 oven for 24 h.

4.2.2. Trypanocidal Action of Compounds **15–18** and **20**

The action of the 3,4,5-trimethoxybenzoic acid derivatives (**15–18** and **20**) against epimastigotes and trypomastigote forms of *T. cruzi* (strain Y) and in host LLC-MK2 cell was evaluated after 24 h of exposure to different concentrations: 100; 50; 25; 12.5; 6.25; 3.12; and 1.56 μg/mL. Cells treated with sterile PBS were considered negative controls (100% viability). The MTT assay was used to determine the cell viability and IC_{50} of the tested substances.

4.2.3. Cell Death Pathway

To assess the cell death pathway was used fluorescence markers 7-aminoactinomycin (7AAD) and annexin V-phycoerythrin (V-PE)., The epimastigote forms of *T. cruzi* were divided into four cell populations: viable cells, with low levels of labeling for both fluorochromes (un-labeled); necrotic cells, labeled only with 7-AAD (7AAD+); apoptotic cells, labeled with annexin V-PE only (AxPE+); and doubly labeled late apoptotic cells (7AAD+/AxPE+) [16]. Epimastigote forms were incubated with compounds **15–18** and **20** for 24 h at concentrations equivalent to IC_{50} and $2 \times IC_{50}$.

4.2.4. Measurement of the Mitochondrial Transmembrane Potential

Evaluation of the mitochondrial transmembrane potential ($\Delta\Psi$m) was performed using Rhodamine 123 (Rho123) (MERCK®, Darmstadt, Germany) cationic dye. At physiological pH, Rho123 is strongly attracted by the negative electrical potential of the mitochondrial inter-membrane space, where it emits red fluorescence [34,35].

4.3. In Silico Study
4.3.1. Molecular Targets

Potential molecular targets for compound **17** in *T. cruzi* were predicted following the homology-based target fishing approach described in previous publications [36]. In summary, the potential targets were identified with the Similarity Ensemble Approach (SEA) method [37]. Next, the SEA-predicted targets for compound **17** were used as queries in a Blast [38] search against the *T. cruzi* (taxid: 5693) proteins included in the Reference proteins (refseq_protein) database. Proteins from *T. cruzi* covered in at least 75% of their length by the Blast alignment and identical in a minimum of 40% to any of the SEA-identified proteins were considered as potential targets of compound **17** in the *T. cruzi*.

4.3.2. Molecular Docking

OpenEye's Omega [39,40] was used to generate one initial three-dimensional conformation of compound **17**. The program MolCharge [41] was used to assign am1bcc partial atomic charges to this ligand conformer. The experimental three-dimensional structures of the DHFR–TS and PPD enzymes were retrieved from the Protein Data Bank (PDB)

database. The PDB codes for these proteins are 3HBB (DHFR–TS) and 3V94 (PPD). Any non-terminal loops missing in the X-ray structures were reconstructed with Modeller [42] using its interface implemented in UCSF Chimera [19]. For the rest of the investigated proteins, no experimental structures were available, and homology models were produced with the SwissModel web server [43]. Different structures, employing different templates, were predicted for every sequence and the model with the highest value of the QMEANDisCo Global metric.

The Gold software [44] was used to perform molecular docking calculations according to the previously described methodology [14]. The ligands present in the experimental X-ray structures and in the templates used for obtaining the homology models were employed to define the receptors' binding regions. Any mechanistically relevant cofactor was retained in the receptors, and hydrogen atoms were added to the proteins prior to docking calculations. The search efficiency parameter in Gold was set to 200%, and up to 10 side chains pointing toward the binding cavity were considered as flexible. The ChemPLP scoring function was used for primary scoring. A total of 30 diverse docking solutions of compound **17** were explored for each receptor, which were later rescored with the Gold's GoldScore, ChemScore, and ASP scoring functions. Finally, the four scoring functions were transformed into Z-scores and averaged at a docking solution level. Any predicted ligand poses with a Z-score larger than 1 were selected for additional analyses.

4.3.3. Molecular Dynamics Simulations and Free Energies of Binding

Amber 2022 [45] was employed for molecular dynamics (MD) simulations as previously described elsewhere [36]. Briefly, all analyzed complexes underwent the same energy minimization, heating, equilibration, and production runs protocol. Proteins were parameterized with the ff19SB force field, and parameters for compound **17** were obtained with the gaff2 force field. Parameters for the NADP cofactor present in the bifunctional DHFR–TS enzyme were retrieved from the Amber parameter database maintained by the Bryce Group at The University of Manchester (http://amber.manchester.ac.uk/index.html, accessed on 16 February 2023). The Zn^{2+} cations present in the HDAC and PPD proteins were parameterized using the cationic dummy atom (CADA) method [46,47]. The receptor–compound **17** complexes were enclosed in truncated octahedron boxes, solvated with water molecules of type OPC, and neutralized by adding Na^+ and Cl^- counterions at a concentration of 150 mM. A first step of energy minimization was then performed with everything except the solvent and counterions constrained. This was followed by a second energy minimization step with no constraints applied. Afterward, the complexes were gradually heated from 0 K to 300 K at constant volume for 20 ps. The heated systems were next equilibrated for 100 ps at constant temperature (300 K) and pressure (1 bar). The equilibrated systems were the starting point for the production runs. Five different short (4 ns) production runs were carried out per complex. Each production run was initialized with random initial atomic velocities for a better exploration of each complex's conformational space.

Free energies of binding were computed from the MD production trajectories with the MM-PBSA method as implemented in the MMPBSA.py script [48] provided with Amber 2022. Calculations took place over 100 MD snapshots extracted from every production run and covering the 1–4 ns time interval. That is, 20 MD snapshots were extracted from each production trajectory for MM-PBSA calculations. The ionic strength for estimating the free energies of binding was set to 150 mM, and default implicit solvent parameters were employed.

5. Conclusions

A series of 3,4,5-trimethoxybenzoic acid derivatives were synthesized, and their SARs were evaluated with respect to trypanocidal activity. It was observed that the amides were more promising than the ester derivatives. Of the compounds tested, the derivative with the highest potency was the amide *N-iso*-butyl-3,4,5–trimethoxybenzamide (**17**) with an IC_{50} = 2.21 μM against the trypomastigote form, an IC_{50} = 8.71 μM for the epimastigote

form from *T. cruzi*, and selectivity of 298.64. The in silico study suggests that the main target of **17** would be HDAC. It was predicted that compound **17** can interact favorably with HDCA by π–π stacking, electrostatic, and hydrogen bond interactions, thus potentially explaining the inhibitory effect of this molecule.

Supplementary Materials: The following supporting information can be downloaded at https://www.mdpi.com/article/10.3390/app132011585/s1. Table S1: Predicted free energies of binding according to the MM-PBSA method; Figures S1–S4: RMSD of compound **17** relative to its docking pose along the MD simulations.

Author Contributions: Execution of the chemical methodology, R.H.N.S. and R.C.G.; execution of the biological methodology, E.P.M.; investigation and writing—original draft preparation, R.H.N.S. and E.PM.; execution of the in silico methodology, Y.P.-C.; data curation, A.M.C.M.; writing—review and editing, and supervision, D.P.d.S. All authors have read and agreed to the published version of the manuscript.

Institutional Review Board Statement: Not applicable.

Informed Consent Statement: Not applicable.

Data Availability Statement: The data presented in this study are available on request from the corresponding author.

Conflicts of Interest: The authors declare that they have no conflict of interest.

Sample Availability: Samples of the compounds are available from the authors.

References

1. Winkler, A.S.; Klohe, K.; Schmidt, V.; Haavardsson, I.; Abraham, A.; Prodjinotho, U.F.; Ngowi, B.; Sikasunge, C.; Noormahomed, E.; Amuasi, J.; et al. Neglected tropical diseases—The present and the future. *Tidsskr. Nor. Laegeforen* **2018**, *2*, 138. [CrossRef] [PubMed]
2. Molyneux, D.H.; Savioli, L.; Engels, D. Neglected tropical diseases: Progress towards addressing the chronic pandemic. *Lancet* **2017**, *389*, 312–325. [CrossRef]
3. Chao, C.; Leone, J.L.; Vigliano, C.A. Chagas disease: Historic perspective. *Mol. Basis Dis.* **2020**, *1866*, 165689. [CrossRef]
4. World Health Organization (WHO). Available online: https://www.who.int/health-topics/chagas-disease#tab=tab_1 (accessed on 27 October 2021).
5. Kropf, S.P. *Chagas Disease, Disease in Brazil: Science, Health and Nation, 1909–1962*; Fiocruz Publisher: Rio de Janeiro, Brazil, 2009; pp. 1–600.
6. Rassi, A., Jr.; Rassi, A.; Marin-Neto, J.A. Chagas disease. *Lancet* **2010**, *375*, 1388–1402. [CrossRef] [PubMed]
7. Souza, W.D. Structural organization of *Trypanosoma cruzi*. *Mem. Oswaldo Cruz Inst.* **2009**, *104* (Suppl. S1), 89–100. [CrossRef] [PubMed]
8. Mesa-Arciniegas, P.; Parra-Henao, G.; Carrión-Bonifacio, Á.; Casas-Cruz, A.; Patiño-Cuellar, A.; Díaz-Rodríguez, K.; Garzón-Jiménez, S.; Almansa-Manrique, J.; Bernal-Rosas, Y.; Hernández-Lamus, C.; et al. *Trypanosoma cruzi* infection in naturally infected dogs from an endemic region of Cundinamarca, Colombia. *Veter Parasitol. Reg. Stud. Rep.* **2018**, *14*, 212–216. [CrossRef]
9. Pérez-Molina, J.A.; Molina, I. Chagas disease. *Lancet* **2018**, *391*, 82–94. [CrossRef]
10. Nóbrega, F.R.; Silva, L.V.; Bezerra Filho, C.D.; Lima, T.C.; Castillo, Y.P.; Bezerra, D.P.; Lima, T.K.; Sousa, D.P. Design, Antileishmanial Activity, and QSAR Studies of a Series of Piplartine Analogues. *J. Chem.* **2019**, *2019*, 1–12. [CrossRef]
11. Silva, R.H.N.; Machado, T.Q.; da Fonseca, A.C.C.; Tejera, E.; Perez-Castillo, Y.; Robbs, B.K.; de Sousa, D.P. Molecular Modeling and In Vitro Evaluation of Piplartine Analogs against Oral Squamous Cell Carcinoma. *Molecules* **2023**, *28*, 1675. [CrossRef]
12. Regasini, L.O.; Cotinguiba, F.; Morandim, A.D.A.; Kato, M.J.; Scorzoni, L.; Mendes-Giannini, M.J.; Bolzani, V.S.; Furlan, M. Antimicrobial activity of Piper arboretum and *Piper tuberculatum* (Piperaceae) against opportunistic yeasts. *Afr. J. Biotechnol.* **2009**, *8*, 2866–2870.
13. Bezerra, D.P.; Pessoa, C.; de Moraes, M.O.; Saker-Neto, N.; Silveira, E.R.; Costa-Lotufo, L.V. Overview of the therapeutic potential of piplartine (piperlongumine). *Eur. J. Pharm. Sci.* **2013**, *48*, 453–463. [CrossRef]
14. Lopes, S.P.; Castillo, Y.P.; Monteiro, M.L.; de Menezes, R.R.; Almeida, R.N.; Martins, A.; Sousa, D.P. Trypanocidal mechanism of action and in silico studies of *p*-coumaric acid derivatives. *Int. J. Mol. Sci.* **2019**, *20*, 5916. [CrossRef] [PubMed]

15. Steverding, D.; da Nóbrega, F.R.; Rushworth, S.A.; de Sousa, D.P. Trypanocidal and cysteine protease inhibitory activity of isopentyl caffeate is not linked in *Trypanosoma brucei*. *Parasitol. Res.* **2016**, *115*, 4397–4403. [CrossRef] [PubMed]

16. Kumar, G.; Degheidy, H.; Casey, B.J.; Goering, P.L. Flow cytometry evaluation of in vitro cellular necrosis and apoptosis induced by silver nanoparticles. *Food Chem. Toxicol.* **2015**, *85*, 45–51. [CrossRef] [PubMed]

17. Krysko, D.V.; Berghe, T.V.; D'herde, K.; Vandenabeele, P. Apoptosis and necrosis: Detection, discrimination and phagocytosis. *Methods* **2008**, *44*, 205–221. [CrossRef] [PubMed]

18. Escudero-Martínez, J.M.; Pérez-Pertejo, Y.; Reguera, R.M.; Castro, M.; Rojo, M.V.; Santiago, C.; Abad, A.; García, P.A.; López-Pérez, J.L.; Feliciano, A.S.; et al. Antileishmanial activity and tubulin polymerization inhibition of podophyllotoxin derivatives on *Leishmania infantum*. *Int. J. Parasitol. Drugs Drug Resist.* **2017**, *7*, 272–285. [CrossRef]

19. Pettersen, E.F.; Goddard, T.D.; Huang, C.C.; Couch, G.S.; Greenblatt, D.M.; Meng, E.C.; Ferrin, T.E. UCSF Chimera—A visualization system for exploratory research and analysis. *J. Comput. Chem.* **2004**, *5*, 1605–1612. [CrossRef]

20. Laskowski, R.A.; Swindells, M.B. LigPlot+: Multiple ligand-protein interaction diagrams for drug discovery. *J. Chem. Inf. Model.* **2011**, *24*, 2778–2786. [CrossRef]

21. Daina, A.; Michielin, O.; Zoete, V. SwissADME: A free web tool to evaluate pharmacokinetics, drug-likeness and medicinal chemistry friendliness of small molecules. *Sci. Rep.* **2017**, *7*, 42717. [CrossRef]

22. Mengarda, A.; Mendonça, P.S.; Morais, C.S.; Cogo, R.M.; Mazloum, S.F.; Salvadori, M.C.; Teixeira, F.S.; Morais, T.R.; Antar, G.M.; Lago, J.H.G.; et al. Antiparasitic activity of piplartine (piperlongumine) in a mouse model of schistosomiasis. *Acta Tropica.* **2020**, *205*, 105350. [CrossRef]

23. Cotinguiba, F.; Regasini, L.O.; da Silva Bolzani, V.; Debonsi, H.M.; Passerini, G.D.; Cicarelli, R.M.B.; Kato, M.J.; Furlan, M. Piperamides and their derivatives as potential anti-trypanosomal agents. *Med. Chem. Res.* **2009**, *18*, 703–711. [CrossRef]

24. A Zuma, A.; de Souza, W. Histone deacetylases as targets for antitrypanosomal drugs. *Future Sci. OA* **2018**, *4*, FSO325. [CrossRef] [PubMed]

25. Di Bello, E.; Noce, B.; Fioravanti, R.; Zwergel, C.; Valente, S.; Rotili, D.; Fianco, G.; Trisciuoglio, D.; Mourão, M.M.; Sales, P.; et al. Effects of Structurally Different HDAC Inhibitors against *Trypanosoma cruzi*, *Leishmania*, and *Schistosoma mansoni*. *ACS Infect. Dis.* **2022**, *8*, 1356–1366. [CrossRef] [PubMed]

26. Da Nóbrega, F.R.; Ozdemir, O.; Sousa, S.C.S.N.; Barboza, J.N.; Turkez, H.; De Sousa, D.P. Piplartine Analogues and Cytotoxic Evaluation against Glioblastoma. *Molecules* **2018**, *23*, 1382. [CrossRef]

27. Green, R.A.; Pletcher, D.; Leach, S.G.; Brown, R.C.D. N-Heterocyclic Carbene-Mediated Oxidative Electrosynthesis of Esters in a Microflow Cell. *Org. Lett.* **2015**, *17*, 3290–3293. [CrossRef] [PubMed]

28. Iranpoor, N.; Firouzabadi, H.; Riazi, A.; Pedrood, K. Regioselective hydrocarbonylation of phenylacetylene to α,β-unsaturated esters and thioesters with $Fe(CO)_5$ and $Mo(CO)_6$. *J. Organomet. Chem.* **2016**, *822*, 67–73. [CrossRef]

29. Nareddy, P.; Jordan, F.; Brenner-Moyer, S.E.; Szostak, M. Ruthenium (II)-catalyzed regioselective C–H arylation of cyclic and N, N-dialkyl benzamides with boronic acids by weak coordination. *ACS Catal.* **2016**, *6*, 4755–4759. [CrossRef]

30. Zinchenko, A.N.; Muzychka, L.V.; Smolii, O.; Bdzhola, V.G.; Protopopov, M.V.; Yarmoluk, S.M. Synthesis and biological evaluation of novel amino-substituted derivatives of pyrido [2,3-d]pyrimidine as inhibitors of protein kinase CK2. *Biopolym. Cell* **2017**, *33*, 367–378. [CrossRef]

31. Obrecht, D.; Bohdal, U.; Broger, C.; Bur, D.; Lehmann, C.; Ruffieux, R.; Schönholzer, P.; Spiegler, C.; Müller, K. L-Phenylalanine Cyclohexyl amide: A simple and convenient auxiliary for the synthesis of optically pure α,α-disubstituted (R)- and (S)-amino acids. *Helv. Chim. Acta* **1995**, *78*, 563–580. [CrossRef]

32. Araújo-Jorge, T.C.; De Castro, S.L. *Design of Experiments and Choice of Models: Host and Parasite. Chagas Disease: Manual for Animal Experimentation*; Fiocruz Publisher: Rio de Janeiro, Brazil, 2000; pp. 175–196.

33. Lima, D.B.; Sousa, P.L.; Torres, A.F.C.; Rodrigues, K.A.d.F.; Mello, C.P.; de Menezes, R.R.P.P.B.; Tessarolo, L.D.; Quinet, Y.P.; de Oliveira, M.R.; Martins, A.M.C. Antiparasitic effect of Dinoponera quadriceps giant ant venom. *Toxicon* **2016**, *120*, 128–132. [CrossRef]

34. Johnson, L.V.; Walsh, M.L.; Chen, L.B. Localization of mitochondria in living cells with rhodamine 123. *Proc. Natl. Acad. Sci. USA* **1980**, *77*, 990–994. [CrossRef] [PubMed]

35. O'Connor, J.E.; Vargas, J.L.; Kimler, B.F.; Hernandez-Yago, J.; Grisolia, S. Use of rhodamine 123 to investigate alterations in mitochondrial activity in isolated mouse liver mitochondria. *Biochem. Biophys. Res. Commun.* **1988**, *151*, 568–573. [CrossRef]

36. Filho, C.S.M.B.; de Menezes, R.R.P.P.B.; Magalhães, E.P.; Castillo, Y.P.; Martins, A.M.C.; de Sousa, D.P. Piplartine-Inspired 3,4,5-Trimethoxycinnamates: Trypanocidal, Mechanism of Action, and In Silico Evaluation. *Molecules* **2023**, *28*, 4512. [CrossRef]

37. Keiser, M.J.; Roth, B.L.; Armbruster, B.N.; Ernsberger, P.; Irwin, J.J.; Shoichet, B.K. Relating protein pharmacology by ligand chemistry. *Nat. Biotechnol.* **2007**, *25*, 197–206. [CrossRef]

38. Altschul, S.F.; Madden, T.L.; Schäffer, A.A.; Zhang, J.; Zhang, Z.; Miller, W.; Lipman, D.J. Gapped BLAST and PSI-BLAST: A new generation of protein database search programs. *Nucleic Acids Res.* **1997**, *25*, 3389–3402. [CrossRef] [PubMed]

39. OMEGA. Open Eye Scientific Software, Santa Fe, NM, USA. Available online: https://www.eyesopen.com/omega (accessed on 16 February 2023).

40. Hawkins, P.C.D.; Skillman, A.G.; Warren, G.L.; Ellingson, B.A.; Stahl, M.T. Conformer generation with OMEGA: Algorithm and validation using high quality structures from the Protein Databank and Cambridge Structural Database. *J. Chem. Inf. Model.* **2010**, *50*, 572–584. [CrossRef] [PubMed]

41. QUACPAC. Open Eye Scientific Software, Santa Fe, NM, USA. Available online: https://www.eyesopen.com/quacpac (accessed on 16 February 2023).
42. Webb, B.; Sali, A. Comparative Protein Structure Modeling Using MODELLER. *Curr. Protoc. Bioinform.* **2016**, *54*, 5.6.1–5.6.37. [CrossRef]
43. Bienert, S.; Waterhouse, A.; de Beer, T.A.P.; Tauriello, G.; Studer, G.; Bordoli, L.; Schwede, T. The SWISS-MODEL Repository-new features and functionality. *Nucleic Acids Res.* **2017**, *45*, D313–D319. [CrossRef] [PubMed]
44. Jones, G.; Willett, P.; Glen, R.C.; Leach, A.R.; Taylor, R. Development and validation of a genetic algorithm for flexible docking. *J. Mol. Biol.* **1997**, *267*, 727–748. [CrossRef]
45. Case, D.A.; Aktulga, H.M.; Belfon, K.; Ben-Shalom, I.Y.; Berryman, J.T.; Brozell, S.R.; Cerutti, D.S.; Cheatham, T.E.; Cisneros, G.A., III; Cruzeiro, V.W.D.; et al. *AMBER 2022*; University of California: San Francisco, CA, USA, 2022.
46. Pang, Y.P.; Xu, K.; E Yazal, J.; Prendergas, F.G. Successful molecular dynamics simulation of the zinc-bound farnesyltransferase using the cationic dummy atom approach. *Protein Sci.* **2000**, *9*, 1857–1865.
47. Pang, Y.-P. Novel Zinc Protein Molecular Dynamics Simulations: Steps Toward Antiangiogenesis for Cancer Treatment. *J. Mol. Model.* **1999**, *5*, 196–202. [CrossRef]
48. Miller, B.R., 3rd; McGee, T.D., Jr.; Swails, J.M.; Homeyer, N.; Gohlke, H.; Roitberg, A.E. MMPBSA.py: An Efficient Program for End-State Free Energy Calculations. *J. Chem. Theory Comput.* **2012**, *8*, 3314–3321. [CrossRef] [PubMed]